Band dispersion of MgB_2, graphite and diamond from resonant inelastic scattering

2003 J. Phys.: Condens. Matter 15 2081

(http://iopscience.iop.org/0953-8984/15/12/325)

INSTITUTE OF PHYSICS PUBLISHING JOURNAL OF PHYSICS: CONDENSED MATTER

J. Phys.: Condens. Matter **15** (2003) 2081–2089 PII: S0953-8984(03)57826-2

Band dispersion of MgB_2, graphite and diamond from resonant inelastic scattering

A V Sokolov[1], E Z Kurmaev[1], S Leitch[2], A Moewes[2], J Kortus[3], L D Finkelstein[1], N A Skorikov[1], C Xiao[2] and A Hirose[2]

[1] Institute of Metal Physics, Russian Academy of Sciences—Ural Division, 620219 Yekaterinburg GSP-170, Russia
[2] Department of Physics and Engineering Physics, University of Saskatchewan, 116 Science Place, Saskatoon, Saskatchewan S7N 5E2, Canada
[3] MPI für Festkörperforschung, Heisenbergstraße 1, D-70569 Stuttgart, Germany

Received 3 January 2003
Published 17 March 2003
Online at stacks.iop.org/JPhysCM/15/2081

Abstract

The quantitative band mapping for MgB_2, graphite and diamond are realized using resonant inelastic x-ray scattering (RIXS) measurements. RIXS shows distinct dispersive features when the excitation energy is tuned near B 1s and C 1s thresholds, which are assigned to the calculated energy bands using $\vec{k}$-momentum conservation. The agreement between experiment and theory suggests that electron–electron interactions are not important for MgB_2, which behaves like a conventional metal and is well described by band theory.

The progress in resonant inelastic x-ray scattering (RIXS) made over recent years allows use of this method, as an alternative technique to angle-resolved ultraviolet photoemission (ARUPS), to perform quantitative band mapping of crystals [1]. RIXS is applicable to many materials that are difficult or impossible to study by angle-resolved photoemission spectroscopy (ARPES), such as insulators and polycrystalline materials. Due to the different excitation and relaxation processes and their corresponding selection rules, RIXS also provides information that is complementary to the well established ARPES. A disadvantage of RIXS is the fact that $\vec{k}$-selectivity is given indirectly and depends on the dispersion of the unoccupied bands. Only at special points, such as band edges and high-symmetry points, can $\vec{k}$ be determined unambiguously using the inelastic scattering experiment.

It has been shown that the carbon Kα x-ray emission spectra (XES) of diamond strongly depend on the excitation energy [2]. Based on this information, it was concluded that the absorption and emission should be treated as a single inelastic scattering process with well defined crystal momentum conservation for photoelectrons and valence band holes. In other words, upon excitation of a core electron to the conduction band (with a certain crystal momentum, based on incident photon energy), emission from the valence band at the same point in the Brillouin zone (same $\vec{k}$-vector) will take place.

0953-8984/03/122081+09$30.00

Ma *et al* [2] showed that carbon Kα XES of diamond strongly depends on the energy of the exciting photons. Based on these results, it is supposed that the absorption–emission process should be treated as a single inelastic scattering process with well defined crystal momentum conservation for photoelectrons and holes in the valence band. This means that when a core electron is promoted to the conduction band with a certain crystal momentum which depends on the incident photon energy, an emission from the valence band at the same point in the Brillouin zone will be induced. The calculation of XES of diamond for different excitation energies using $\vec{k}$-momentum conservation has shown a good agreement with experiments [2, 3]. Similar calculations performed for graphite [4, 5] and for cubic and hexagonal BN [3] have also shown a reasonable agreement between calculated and experimental spectra. Using RIXS measurements as a method of quantitative band mapping was first demonstrated for SiC by Lüning *et al* [6].

In this paper we demonstrate quantitative band mapping for diamond, graphite and MgB_2 using RIXS. The latter, a recently discovered superconductor with $T_c = 39$ K [7], is of greatest interest. Only small ($0.3 \times 0.3 \times 0.1$ mm^3) single crystals of this compound are currently available [8, 9], making ARUPS measurements very difficult. Consequently, because of contrast problems due to low intensity (and large background) arising from the small crystal, the first ARUPS measurements [10] did not reveal clear dispersion for normal emission. The authors of this paper found the electronic state centred at the Γ point which does not correspond to any predicted bulk band structure and is attributed to a surface electronic state due to the extreme surface sensitivity of the angular resolved photoemission measurements. The observed B isotope shift of T_c [11] indicates that pairing in MgB_2 is due to phonons. An evaluation of the electron–phonon coupling shows that it is strong enough for the appearance of a surprisingly high transition temperature [12, 13]. The isotope effect probes the extent to which phonons mediate superconductivity. In the classical form of the Bardeen–Cooper–Schrieffer (BCS) theory the isotope coefficient α, defined by the relation $T_c \propto M^{-\alpha}$ (M—mass of the element), is equal to 1/2. According to [11], the boron isotope exponent can be estimated as 0.26 which is close to those obtained for borocarbides YNi_2B_2C and $LuNi_2B_2C$ where theoretical works suggested that the phonons (boron A_{1g} optical modes) are responsible for the superconductivity. It has been also suggested that electron–electron correlations can be responsible for an increase of the superconducting temperature [14]. These open questions make studies of the electronic structure of MgB_2 worthwhile.

We have used a self-consistent linearized muffin-tin orbital (LMTO) method within the local density approximation (TBLMTO-47 computer code [16]) and the FLAPW WIEN97 code [17] for our band structure calculations.

Soft x-ray fluorescence measurements of polycrystalline diamond, MgB_2 and highly oriented pyrolytic graphite (HOPG) were performed at Beamline 8.0.1 of the Advanced Light Source at Lawrence Berkeley National Laboratory and its soft x-ray fluorescence endstation [15]. The emitted radiation is partially recorded in a Rowland circle-type spectrometer with spherical gratings and an area-sensitive multichannel detector. This combination provides an instrumental resolution of about 0.3 eV at C and B Kα emission energies. All emission spectra are normalized to the number of photons falling on the sample monitored by a gold mesh in front of the sample.

The MgB_2 sample was prepared from powdered magnesium (Mg; 99.9%) and powdered amorphous boron (B; 99%) in a dry box. The powders were mixed in an appropriate ratio (Mg:B = 1:2), ground, pressed into pellets and heated at 973 K under a high argon pressure, 196 MPa, using a hot isostatic pressing furnace for 10 h.

The general procedure for RIXS experiments consists of measuring the x-ray absorption spectrum (XAS) in the total electron yield (TEY) mode. The emission spectra (XES) are then

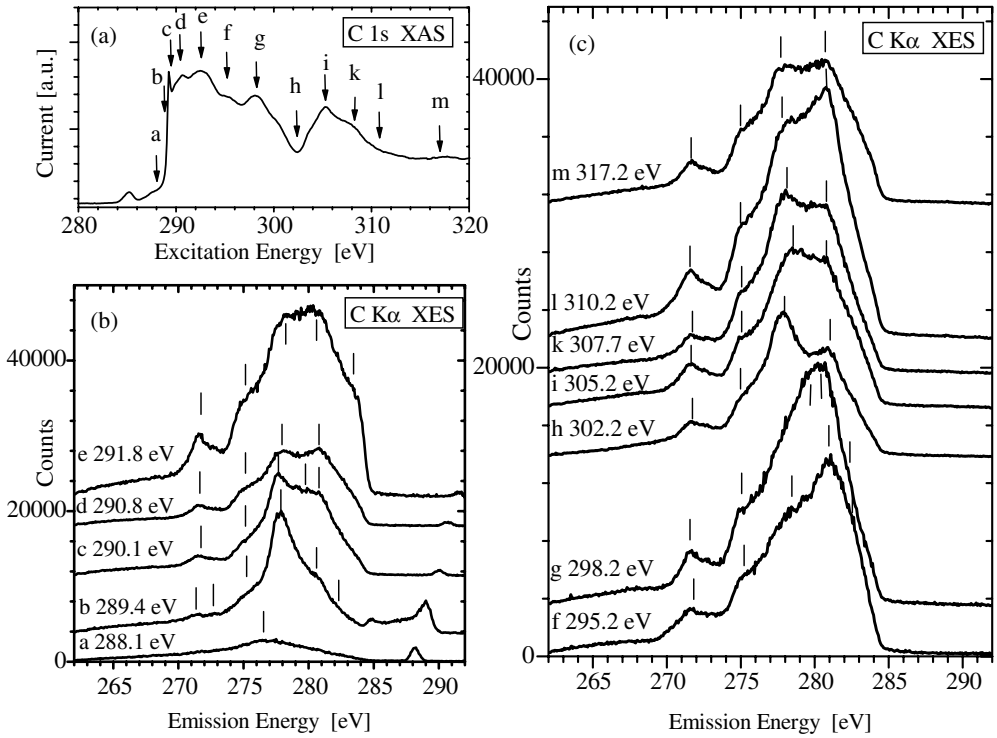

Figure 1. C 1s XAS of diamond (a) and C Kα XES of diamond measured at selected excitation energies in the vicinity of the C 1s threshold (b) and (c).

recorded at selected excitation energies. The excitation energy is tuned through the respective B and C 1s thresholds.

In the RIXS band mapping procedure [1], excitation energies for the emission spectra are selected at spectral features in the absorption spectrum, which correspond to points of high symmetry in the Brillouin zone. We therefore measured C and B 1s absorption spectra of diamond, graphite and MgB_2 in order to select the appropriate excitation energies for the emission spectra. The Kα emission spectra ($2p \rightarrow 1s$ transition) were recorded at those selected excitation energies. Strong dispersion of the C emission spectra is observed in figures 1(b) and (c). This procedure does not take into account points between those of high symmetry. So, in order to include a larger number of points along the dispersion curves in the region of interest (usually 0–20 eV), more excitation energies are selected.

Figure 2 demonstrates, for the emission spectrum excited at 289.4 eV, how we obtain experimental points on the dispersion curves. The top of the valence band corresponds to zero on the energy scale, which is related to an XPS C 1s binding energy, for diamond, of 284.5 eV [18]. In figure 2(b), the solid horizontal line, corresponding to the excitation energy, crosses the 2p dispersion curves for unoccupied states at three points. These points determine the possible values of $\vec{k}$ that will induce a C $1s \rightarrow 2p$ transition. Then, using $\vec{k}$-momentum conservation, the vertical lines from the intersection points are drawn down to the dispersion curves for occupied states.

Features of the carbon Kα XES reveal the location of occupied states. To assure the accuracy of occupied state feature selection, the first derivative of the XES was calculated with

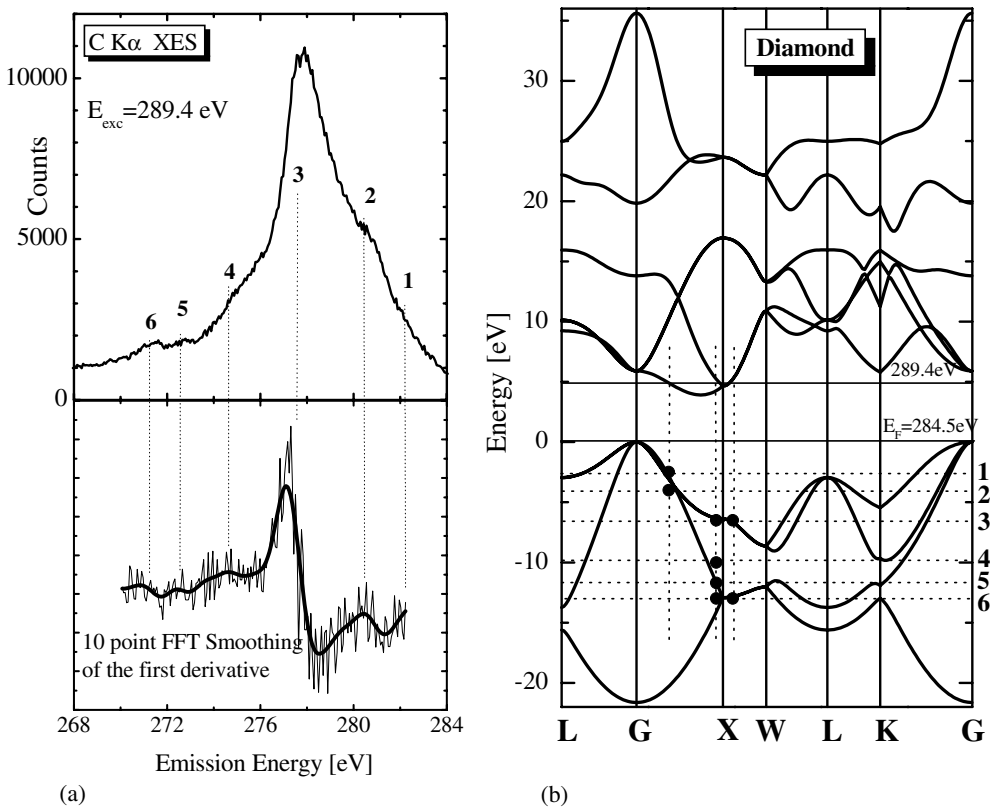

Figure 2. (a) C Kα XES of diamond measured at $E_{exc} = 289.4$ eV (upper panel) and 10-point FFT smoothing of the first derivative (lower panel). (b) The comparison of calculated and experimental dispersion curves based on the treatment of the C Kα XES of diamond measured at $E_{exc} = 289.4$ eV.

10-point FFT smoothing (figure 2(a)). Six features can be distinguished for C Kα XES with excitation energy $E_{exc} = 289.4$ eV (figure 2(a)). The horizontal dotted lines in figure 2(b) correspond to those features.

The intersection points of horizontal and vertical dotted lines give the experimental points on the dispersion curves for occupied states. If the band structure calculation is correct, each experimental point will be situated near the calculated dispersion curve for at least one possible $\vec{k}$-value. This procedure was used for emission spectra excited at all excitation energies. The obtained results (figure 3) show a good agreement between experimental and calculated dispersion curves.

Using the same procedure, experimental dispersion curves were constructed for graphite C 1s (figure 4, $E_{bind} = 284.5$ eV [19]). The measured XES with respect to excitation energy for graphite (figure 4(a)) are in good agreement with experimental spectra, as measured by Carlisle *et al* [20]. The C Kα XES measured at $E_{exc} = 299$ eV (i.e. far above the threshold) represents a non-resonant spectrum which, according to dipole selection rules, probes p ($l = 1$) partial DOS. Under resonant excitation, the emission spectra show features that are changing with excitation energy and can characterize the different types of dispersive features. At low excitation energy ($E_{exc} = 285.0$ eV, figure 4(a)), the peaks located in the energy range of 268–276 eV can be attributed to the lowest part of the σ-states. The peaks at 283 eV are

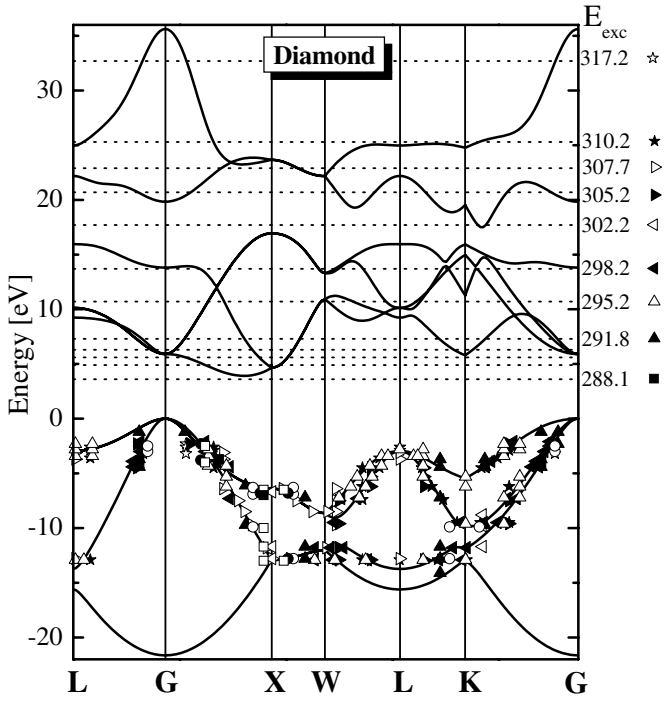

Figure 3. A comparison of experimental and calculated dispersion curves of diamond based on the treatment of experimental spectra presented in figure 1. Each symbol corresponds to one excitation energy as labelled in figure 1.

attributed to π-states. At $E_{exc} = 285.6$ and 288.0 eV, σ-peaks are shifted to higher energies, probing higher parts of the σ-band, while the π-peak is shifted to a lower energy. Beginning at $E_{exc} = 291.3$ eV, the spectra show a weaker dependence on excitation energy. The fine structure develops into the usual spectra observed in the non-resonant case. This interpretation corresponds to orientation-dependent measurements of single-crystal graphite [21], where σ- and π-bands are probed separately. In addition, figure 4(b) shows that the experimental points fit well to the theoretical band structure of graphite.

Using the B 1s ($E_{bind} = 185.5$ eV [22]) XES, quantitative RIXS band mapping of MgB_2 was performed (figure 5). The excitation energy dependence of boron Kα-emission in MgB_2 is less pronounced (figure 5(a)) than that of carbon Kα-emission in graphite (figure 4(a)). This can be explained by band structure calculations (figures 4(b) and 5(b)), in which the Fermi level in MgB_2 is shifted with respect to graphite, crossing the σ-band with a high density of states. As a result, the MgB_2 spectra show mainly occupied σ-states, whereas graphite reveals both σ- and π-states. The position of the Fermi level seems to explain why σ spectral features show a weaker dependence on excitation energy within the σ-band. In graphite, the excitation energy (E_{exc}) is shifted at first along the π-band, whereas in MgB_2, it is immediately on the σ-band, a more favourable condition for excitation. Figure 5(b) shows good agreement between our experimental results and theoretical band structure calculations.

Note that states near the Fermi level have a strong local boron p-character, which supports the idea that the B 2p-states are responsible for the superconductivity in MgB_2. This is the main conclusion of all available band structure calculations.

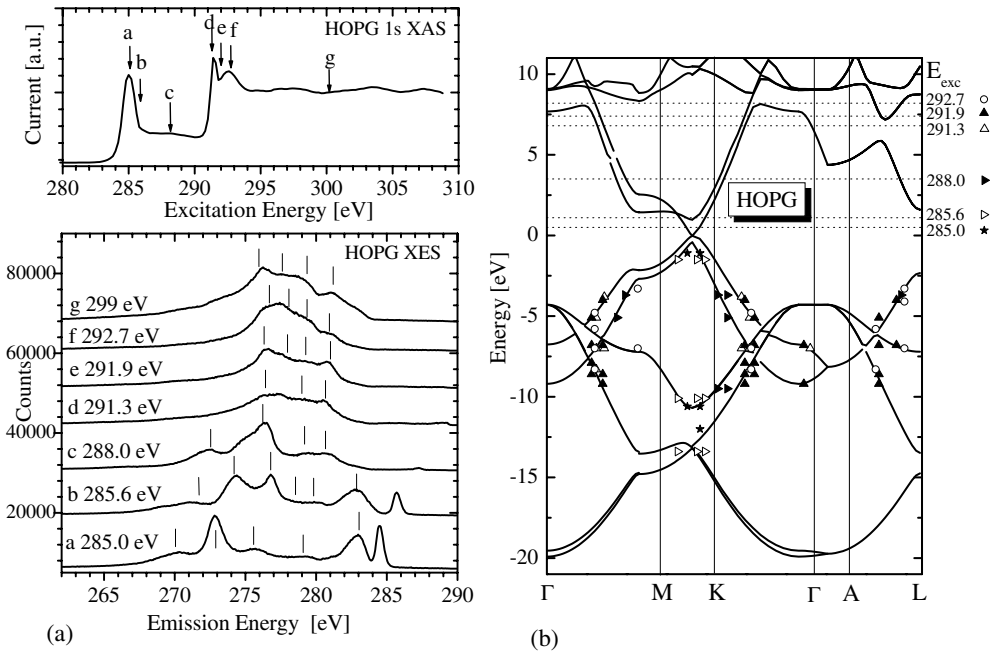

Figure 4. (a) XES dependence on excitation energy of HOPG near the C 1s-threshold excitation. (b) Band mapping using RIXS, curves show the calculated band structure and symbols represent the experimental results for various excitation energies.

The dispersion of the σ-bands near the Fermi level is well reproduced in all directions. This agreement of theory and experiment suggests that electron–electron interactions, beyond the mean-field treatment of these correlations within density functional theory, are not important. MgB_2 behaves like a conventional metal, well described by band theory. This has very important implications on the interpretation of current experimental results. It seems unlikely that a large Coulomb pseudo-potential μ^* is the reason for the observed reduced total isotope effect [23]. Other explanations, such as anharmonicity or non-linear electron–phonon coupling, have yet to be explored.

Optical spectroscopy is also a direct probe of the electronic structure. The reported plasma frequency of approximately 1.5 eV [24] is in utter disagreement with the plasma frequency calculated from the band structure of 7 eV [12, 25]. It would be tempting to ascribe this discrepancy to a failure of band theory due to correlation effects. Our results lend credibility to optical properties calculated from band structure. Inter-band conductivity and other mechanisms have to be investigated in order to explain this discrepancy.

Figures 4 and 5 show that the dispersion of occupied states of graphite and MgB_2 are very similar due to their structural and electron identity. In graphite, σ-bonding states are completely filled, which gives a strong covalency and semi-metallic behaviour. In MgB_2, σ-states are unfilled, providing a higher density of states and metallic properties. According to An and Pickett [26], the attractive potential of Mg^{2+} between B_2 layers lowers the π-bands, inducing $\sigma \rightarrow \pi$ charge transfer which drives the hole doping of the σ-band and provides superconductivity. Recent band structure calculations show a similar effect under hole doping of insulating LiBC (which has the same crystal structure as MgB_2) and predict high-T_c superconductivity with $T_c = 100$ K for $Li_{0.5}BC$ [27]. Based on our RIXS measurements, we

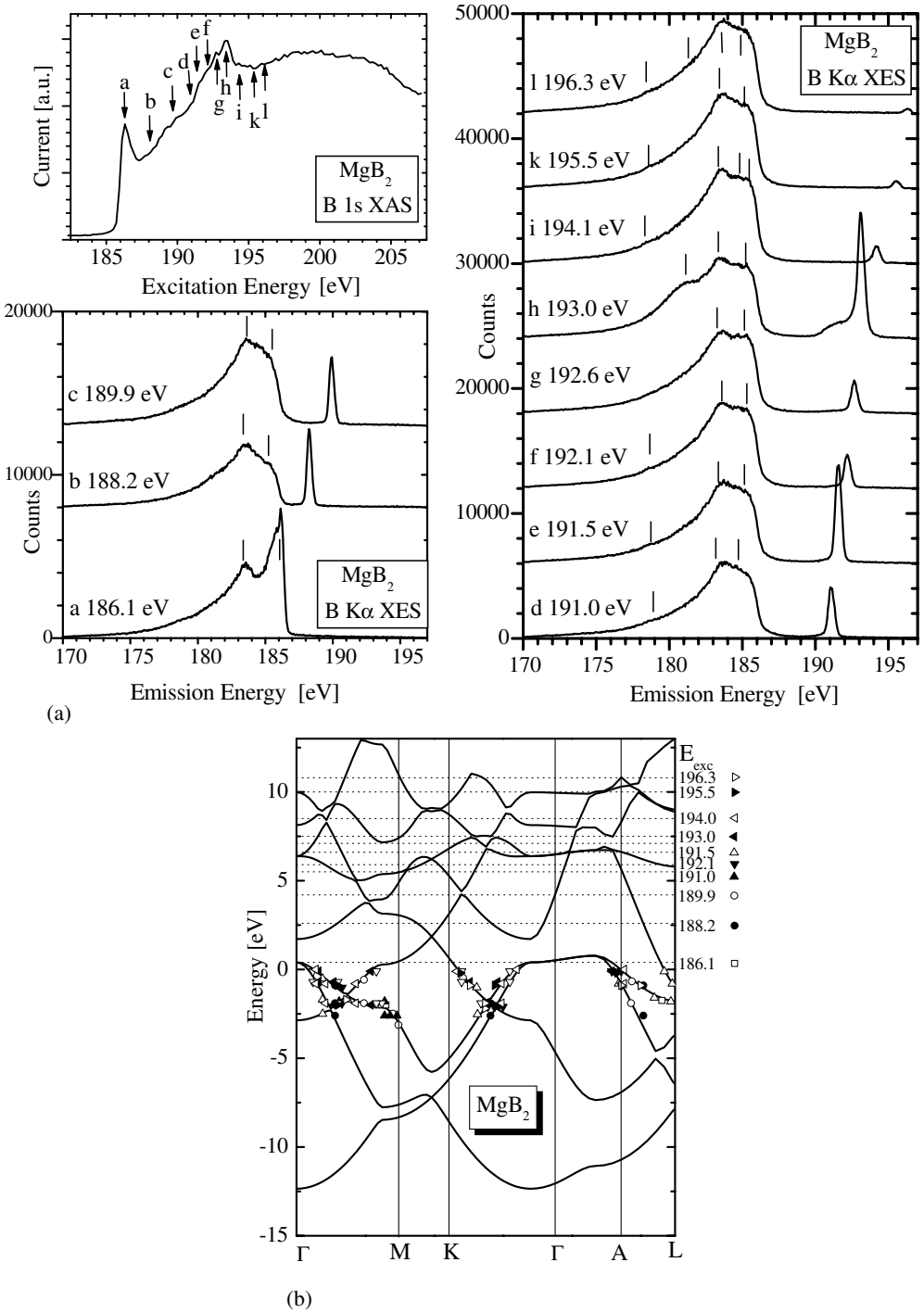

Figure 5. (a) XES dependence on excitation energy of MgB_2 near the B 1s-threshold excitation. (b) Band mapping using RIXS, curves show the calculated band structure and symbols represent the experimental results.

can conclude that experimental dispersion curves of graphite and MgB_2 show the different degrees of filling of the energy bands and thus strongly support the ideas described above.

In conclusion, we have studied band dispersion for MgB_2 and graphite by RIXS focusing, in particular, for $E(\vec{k})$ dispersion curves. We have found good agreement between theory and experiment for all detected dispersive features, which suggests that electron–electron correlations are weak, and the electronic structure of MgB_2 is well described by conventional band theory.

Acknowledgments

Funding by the Russian Foundation for Basic Research (Project 00-15-96575), the Russian State Programme on Superconductivity, Natural Sciences and Engineering Research Council of Canada (NSERC), and the NATO Collaborative Linkage Grant is gratefully acknowledged. The work at the Advanced Light Source at Lawrence Berkeley National Laboratory was supported by US Department of Energy (Contract no DE-AC03-76SF00098). JK would like to thank I I Mazin and O Jepsen for helpful discussions and the Schloeßmann foundation for financial support.

References

[1] Eisebitt S and Eberhardt W 2000 *J. Electron Spectrosc. Relat. Phenom.* **110/111** 335
[2] Ma Y, Wassdahl N, Skytt P, Guo J, Nordgren J, Johnston P D, Rubensson J-E, Boske T, Eberhardt W and Kevan S D 1992 *Phys. Rev. Lett.* **69** 2598
[3] Shirley E L 2000 *J. Electron Spectrosc. Relat. Phenom.* **110/111** 305
[4] Carlisle J A, Shirley E L, Hudson E A, Terminello L J, Callcott T A, Jia J J, Ederer D L, Perera R C C and Himpsel F J 1995 *Phys. Rev. Lett.* **74** 1234
[5] Carlisle J A, Blankenship S K, Terminello L J, Jia J J, Callcott T A, Ederer D L, Perera R C C and Himpsel F J 2000 *J. Electron Spectrosc. Relat. Phenom.* **110/111** 323
[6] Lüning J, Rubensson J-E, Ellmers C, Eisebitt S and Eberhardt W 1997 *Phys. Rev.* B **56** 13147
[7] Nagamatsu J, Nakagawa N, Muranaka T, Zenitani Y and Akimitsu J 2001 *Nature* **410** 63
[8] Xu M, Kitazawa H, Takano Y, Ye J, Nishida K, Abe H, Matsushita A, Tsujii N and Kido G 2001 *Appl. Phys. Lett.* **79** 2779
[9] Eltsev Y, Nakao K, Lee S, Mosui T, Chikumoto N, Tajima S, Koshizuka N and Murakami M 2002 *Phys. Rev.* B **66** 180504
[10] Uchiyama H, Shen K M, Lee S, Damascelli A, Lu D H, Feng D L, Shen Z-X and Tajima S 2002 *Phys. Rev. Lett.* **88** 157002
[11] Bud'ko S L, Lapertot G, Petrovic C, Cunningham C E, Anderson N and Canfield P C 2001 *Phys. Rev. Lett.* **86** 1877
[12] Kortus J, Mazin I I, Belashenko K D, Antropov V P and Boyer L L 2001 *Phys. Rev. Lett.* **86** 4656
[13] Belashenko K D, van Schilfgaarde M and Antropov V P 2001 *Phys. Rev.* B **64** 92503
[14] Hirsch J E 2001 *Phys. Lett.* A **282** 392
[15] Jia J J, Callcott T A, Yurkas J, Ellis A W, Himpsel F J, Samant M G, Stöhr J, Ederer D L, Carlisle J A, Hudson E A, Terminello L J, Shuh D K and Perera R C C 1995 *Rev. Sci. Instrum.* **66** 1394
[16] Anderson O K 1975 *Phys. Rev.* B **12** 3060
[17] Blaha P, Schwarz K and Luitz J 1999 *WIEN97, A Full Potential Linearized Augmented Plane Wave Package for Calculating Crystal Properties* Technical University of Vienna (ISBN 3-9501031-0-4)
This is an improved and updated Unix version of the original copyrighted WIEN code, which was published by Blaha P, Schwarz K, Sorantin P and Trickey S B 1990 *Comput. Phys. Commun.* **59** 399
[18] Moulder J F, Sticle W F, Sobol P E and Bomben K D 1992 *Handbook of X-Ray Photoelectron Spectroscopy* (Eden Praire, MN: Perkin-Elmer Corp.)
[19] Bruhwiller P A 1995 *Phys. Rev. Lett.* **74** 614
[20] Carlisle J A, Shirley E L, Hudson E A, Terminello L J, Callcott T A, Jia J J, Ederer D L, Perera R C C and Himpsel F J 1995 *Phys. Rev. Lett.* **74** 1234
[21] Beyreuther C, Hierl R and Wiech G 1975 *Ber. Bunsenges. Phys. Chem.* **79** 1081

[22] Kurmaev E Z, Lyakhovskaya I I, Kortus J, Moewes A, Miyata N, Demeter M, Neumann M, Yanagihara M, Watanabe M, Muranaka T and Akimitsu J 2002 *Phys. Rev.* B **65** 134509
[23] Hinks D G, Claus H and Jorgensen J D 2001 *Nature* **411** 457
[24] Kaindl R A, Carnahan M A, Orenstein J, Chemla D S, Christen H M, Zhai H-Y, Paranthaman M and Lowdness D H 2002 *Phys. Rev. Lett.* **88** 27003 (*Preprint* cond-mat/0106342)
[25] Liu A Y, Mazin I I and Kortus J 2001 *Phys. Rev. Lett.* **87** 87005
[26] An J M and Pickett W E 2001 *Phys. Rev. Lett.* **86** 4366
[27] Rosener H, Kitaigorodsky A and Pickett W E 2002 *Phys. Rev. Lett.* **88** 127001